Cadmium isotope fractionation during adsorption onto calcite

Huan Peng,[1] Peng Liu,[2, 4] Hongtao Zheng,[3] Nicholas S. Belshaw,[1,5] Shenghong Hu,[1] and Zhenli Zhu[1, 3, 4 *]

[1]State Key Laboratory of Biogeology and Environmental Geology, China University of Geosciences, Wuhan, 430074, China

[2]School of Environmental Studies, China University of Geosciences, Wuhan 430074, China

[3]Faculty of Material Science and Chemistry, China University of Geosciences, Wuhan 430074, China

[4]Hubei Key Laboratory of Yangtze Catchment Environmental Aquatic Science, Wuhan 430074, China

[5]Department of Earth Sciences, Oxford University, Oxford OX1 3PR, United Kingdom

Correspondence and requests for materials should be addressed to:

Dr. Zhenli Zhu, State Key Laboratory of Biogeology and Environmental Geology, China University of Geosciences, Wuhan 430074, China, Email: zlzhu@cug.edu.cn

Abstract:

Adsorption on mineral surfaces is a crucial process controlling (bio)geochemical cycling of Cd in a range of environments. Cd isotopic behaviour during adsorption is an important but little investigated aspect of Cd isotope systematics. This work looked at the fractionation of Cd isotopes during Cd adsorption onto calcite. This is an important sink of Cd but isotopic behaviour has only previously been investigated in co-precipitation experiments. The Cd isotope composition of calcite adsorbed components was determined to be lighter and consistent with equilibrium fractionation in all experiments. The degree of fractionation observed in our experiments is not influenced by the $Cd/CaCO_3$ ratio, pH value or Cd/PO_4^{3-} ratio in the studied range. In MQ water, the observed fractionation value $\alpha_{sorbed\text{-}aqueous}$ is 0.99934 but this α value is affected by the presence of other compounds. Notably, $\alpha_{sorbed\text{-}aqueous}$ = 0.99984, a reduced but resolvably lower value fractionation, was observed in the presence of PO_4^{3-} which may be an important factor to be considered when interpreting Cd isotope signatures in nature. The enrichment of lighter Cd isotopes may result from highly distorted octahedral $Cd\text{-}O_6$ sites of inner-sphere Cd complexes on calcite, indicated by extended X-ray absorption fine structure (EXAFS). The reduced Cd isotope fractionation observed in the presence of PO_4^{3-} may result from near identical coordination environments of the aqueous and sorbed Cd species. This work suggests adsorption of Cd onto carbonates minerals may produce significant Cd isotope fractionation between fluids and solid phase. Our observations offer an alternative process apart from co-precipitation when interpreting Cd isotope

ratios in the presence of calcite in paleo-geological studies and could be helpful to better understand Cd (bio)geochemical cycling.

Key words: cadmium isotope fractionation, calcite, cadmium adsorption, phosphate, EXAFS, cadmium (bio)geochemical cycling

1. Introduction

Carbonate minerals occur ubiquitously in a variety of geochemical environments including sediments, soils, and aquifers, in which calcite is most abundant (Comans and Middelburg, 1987; Martin-Garin et al., 2003; Prieto et al., 2003). Numerous studies have demonstrated the high affinity of divalent cations (e.g., Cd *etc*.) for carbonate minerals leading to their accumulation and preservation, in some case recording environmental information (Brown and Parks, 2001; Comans and Middelburg, 1987; Morse, 1986; Zachara et al., 1991). Carbonate minerals have been extensively used as an important archive to access past environmental information, where associated stable isotope signals could be used as proxies for (bio)geochemical processes or paleo-environmental changes in geological history (Meyer and Kump, 2008; Smrzka et al., 2019; Tribovillard et al., 2006; Zeebe, 2012). For example, Cd isotope signatures in carbonate have been used for anchoring biological extinction events (Zhang et al., 2018), estimating marine primary productivity(Georgiev et al., 2015) and global micronutrient cycles (Sweere et al., 2020).

Measurement of metal or non-metal isotope signals in carbonate minerals requires an understanding of isotope behaviour and fractionation mechanisms which occur during processes leading to the uptake and incorporation of the elements. Knowledge of fractionation factors operating for specific processes are necessary for the use of isotope signatures as process tracers (Wiederhold, 2015). Available studies have shown processes causing Cd retention in carbonate minerals can be generally divided into adsorption (Kozar et al., 1992; Prieto et al., 2003; Shirvani et al., 2006a)

and co-precipitation (Bottcher, 1997; Horner et al., 2011; Xie et al., 2020). These two processes may result in different isotope behaviour during the incorporation of ions into minerals. Generally, equilibrium isotope fractionation is observed during adsorption while kinetic isotope fractionation occurs during co-precipitation. For example, Alvarez *et al.* (2020) noted equilibrium isotope fractionation of $\Delta^{60/58}Ni_{calcite\text{-}fluid}$ = -0.52‰ during adsorption of Ni onto calcite, but later observed that $\Delta^{60/58}Ni_{calcite\text{-}fluid}$ was affected by carbonate growth rate during the co-precipitation of Ni into calcite, and estimated that $\Delta^{60/58}Ni_{calcite\text{-}fluid}$ is < -1.0‰ if equilibrium achieved (Alvarez et al., 2021). Observing different $\Delta^{60/58}Ni_{calcite\text{-}fluid}$ values in adsorption and co-precipitation processes may give helpful insights into oceanic Ni mass balance (Alvarez et al., 2021; Alvarez et al., 2020). Therefore, in order to better investigate (non)metal isotope signals in carbonate minerals, it is crucial to thoroughly evaluate isotope behaviour associated with the uptake of ions by carbonate minerals.

The study of cadmium (Cd) stable isotopes has recently received increasing attention because its variation can provide useful information both for studying aspects of marine biogeochemistry and for tracking natural and anthropogenic attenuation of Cd fluxes in contaminated aquifers (Rehkämper et al., 2011). Sedimentary carbonates are increasingly used as archives for paleo-oceanic studies (Smrzka et al., 2019). Adsorption of Cd onto calcite is recognized to be an important process controlling the mobility and bioavailability of Cd and is invoked as a probable metal-scavenging process in aquatic, marine, and ground-water systems (Brown and Parks, 2001; Hay et al., 2003; Zachara et al., 1991). In addition, Cd isotopes are also

proposed as a potential tracer for determining the extent to which adsorption on mineral substrates affects Cd transport in contaminated aquifers (Wasylenki et al., 2014).

Few experimental studies have investigated Cd isotope behaviour during uptake by calcium carbonate, and all focused only on the process of co-precipitation (Horner et al., 2011; Wombacher et al., 2003; Xie et al., 2020). Wombacher *et al*. (2003) first studied Cd isotope behaviour while co-precipitating with aragonite, and found that Cd in the mineral phase was isotopically light relative to solution Cd. Later, Horner *et al*. (2011) reported that Cd co-precipitating with calcite resulted in no observable Cd isotope fractionation in freshwater but noted fractionation, $\alpha_{\text{calcite-aqueous}}$ of 0.99955 in artificial seawater. More recently, Xie *et al*. (2020) conducted similar research under groundwater conditions and preferential uptake of lighter Cd was similarly observed.

Noting the previous studies, it appears that little effort has been focused on Cd isotope behaviour during adsorption onto calcite even though high affinity and fast adsorption of Cd have been widely reported (Davis et al., 1987; Martin-Garin et al., 2003). Only two works have examined Cd isotope behaviour during adsorption but only with birnessite (Wasylenki et al., 2014) and iron (oxyhydr)oxides (Yan et al., 2021) as adsorbents. The reported preferential enrichment of lighter Cd by these substrates are controlled by Cd species, and appears to follow equilibrium fractionation as opposed to Rayleigh fractionation during (co-)precipitation with minerals (calcite (Horner et al., 2011; Xie et al., 2020) and sulfides (Guinoiseau et al., 2018)). Another reference exists in a conference abstract, also showing kaolinite

preferentially adsorb lighter Cd (Qin et al., 2019). These works highlighted the importance of understanding isotope fractionation during adsorption, needed to better estimate the potential use of Cd isotopes as traces. On the other hand, related studies have looked at isotope fractionation of a number of elements during adsorption onto calcite, including Ga (Yuan et al., 2018), Ni (Alvarez et al., 2020), B (Saldi et al., 2018), and Zn (Dong and Wasylenki, 2016).

In this work, Cd isotope ratios between aqueous Cd and Cd adsorbed onto calcite are measured under different experimental conditions and possible fractionation mechanisms are considered. In addition to typical variates of Cd/calcite ratio and pH value, we further examined effects of some co-existing (in)organics (e.g., PO_4^{3-}) on isotope fractionation during adsorption. The preferential enrichment of lighter Cd in the solid phase is noted during adsorption, and the co-existing (in)organics are observed to alter the degree of Cd isotope fractionation. Notably, the presence of PO_4^{3-} acts to greatly reduce Cd isotope fractionation. Variation of Cd/calcite ratio, pH value, and Cd/PO_4^{3-} ratio are seen to have little influence on Cd isotope fractionation factors ($\alpha_{sorbed\text{-}aqueous}$) in the studied range. Extended X-ray Absorption Fine Structure Spectroscopy (EXAFS) was employed to investigate Cd bonding environments to provide information regarding observed Cd isotope fractionation. This study may contribute to an improved understanding of Cd isotope behaviour during its interaction with mineral surfaces in natural mineral-aqueous environments.

2. Methods and materials

135 **2.1 Starting materials.**

136 Calcium carbonate as adsorbent (99.99%) was obtained from Macklin with its
137 purity confirmed by X-ray diffraction (XRD) (Figure S1). Cadmium nitrate (99.99%),
138 sodium phosphate (99.99%) and sodium citrate (99%) were purchased from Aladdin
139 and 1,3-propanedithiol (99%, -thiol hereafter) was obtained from Sigma-Aldrich.
140 PO_4^{3-}, citrate and -thiol were used as co-existing compounds. The ~50 mmol/L stock
141 solutions of each chemical were prepared with MQ water, and then the mixture of Cd
142 with selected compounds at low concentration were prepared. All the chemicals,
143 consumables and labware cleaning procedure are detailed in Supplementary
144 Information (SI) section 1.

145

146 **2.2 Adsorption experiments**

147 Before conducting batch adsorption experiments, preliminary experiments were
148 carried out and showed neither centrifuge tube walls nor the use of syringe and 0.22
149 μm filters cause aqueous Cd loss and isotope alteration in the studied range.
150 Simulation (Visual MINTEQ 3.1 (Figure S2)) also showed no Cd would be
151 precipitated in the designed range. In addition, centrifuged solids XRD patterns
152 (Figure S1) confirmed no bulk production of Cd precipitates and other Cd-bearing
153 minerals. Thus, all the Cd lost from aqueous solution was ascribed to adsorption onto
154 calcite and Cd isotope fractionation in our experiments is not induced by Cd
155 (co)-precipitation.

156 Batch experiments were performed in centrifuge tubes in which $Cd/CaCO_3$ ratios,

157 solution pH, and Cd/PO_4^{3-} ratios varied independently (Table S1). The pH of all
158 solutions and suspensions were adjusted using 10 mmol/L HCl or NaOH. Calcite
159 suspensions were maintained at target pH values for at least 24 h initially and then Cd
160 and mixed solutions were added as required. Once mixed, centrifuge tubes were
161 sealed and shaken continuously at 60 rpm. After 24 h shaking, each suspension was
162 centrifuged (8000 rpm, 30 min) to separate supernatant and solid, and the former was
163 further filtered by 0.22 μm filters. All the filtrates were stored in a refrigerator before
164 use (both concentration and isotope analysis). For the study of Cd/$CaCO_3$ ratios with
165 the calcite loading of 0.1 - 20 g/L, the final Cd concentration was ~0.5 mmol/L with
166 ~0.1 mmol/L for the co-existing (in)organics. To study the pH dependent adsorption
167 behaviour, the Cd/$CaCO_3$ ratio was fixed at 0.5 : 5.0 (mmol/L : g/L), whilst pH was
168 varied from 5.74 to 8.30. The Cd/PO_4^{3-} ratio dependence was explored using a calcite
169 loading of 1 g/L, whilst the Cd/PO_4^{3-} ratio was varied from 0.25:0.1 to 0.001:0.1
170 (mmol/L : mmol/L).

171 It seems that constraining pCO_2 strictly or not show negligible effect on ion
172 adsorption behavior and corresponding isotope fractionation (Yuan et al., 2018).
173 Therefore, the effect of pCO_2 is not considered in this study, but calcite suspensions
174 and (in)organic solutions were pre-maintained in storage bottles at target pH at
175 atmosphere condition. The pH values were kept constant at least 24 h before
176 conducting experiments and it was measured before and after each adsorption
177 experiment. Adsorption time was set at 24 h according to some previous work
178 (Wasylenki et al., 2014; Yan et al., 2021), where 24 h is sufficient for Cd isotopes to

achieve equilibrium between adsorbed and aqueous species. It should be noted that in this work, pure water without background electrolyte was set as a base. Since chloride present as a background electrolyte could alter hexahydrate Cd ions to Cd-Cl complexes, this would likely affect isotope behaviour during adsorption (Guinoiseau et al., 2018; Wasylenki et al., 2014). In contrast, Cd isotope fractionation is barely affected by ionic strength during adsorption using nitrate as a background electrolyte as the reduced partition function ratio of $Cd(NO_3)(H_2O)_5^+$ is almost equal to $Cd(H_2O)_6^{2+}$ (Yan et al., 2021). Therefore, to simplify the experimental system, no background electrolyte was used.

In this study, sodium phosphate, sodium citrate, and 1,3-propanedithiol were chosen as co-existing compounds to study Cd isotope fractionation during adsorption, since the co-existence of Cd and (in)organics, such as PO_4^{3-}, -thiol, and -carboxyl species, appears to be the case in soils, surface/ground water and marine systems (Boyle et al., 1976; Kubier et al., 2019), and they are certainly coupled to undergo (bio)geochemical cycling (Duhamel et al., 2021). The co-existing (in)organics may alter Cd species which further indeed influence Cd isotope fractionation during adsorption (Collins et al., 1999; Fujii and Albarède, 2012; Wasylenki et al., 2014; Zhao et al., 2021). In addition, we further investigated the effect of Cd/PO_4^{3-} ratio on Cd isotope fractionation because (i) we preliminarily found the presence of PO_4^{3-} acts to greatly reduce Cd isotope fractionation during adsorption, and (ii) distribution of Cd is generally correlates with macronutrient phosphate (PO_4^{3-}), especially in the marine environment, covering a wide range of Cd/PO_4^{3-} ratio.

2.3 Cadmium isotope analysis.

Before isotopic analyses, Cd was purified according to our previous protocol (Peng et al., 2021), which detailed in SI section 2. Briefly, Cd from the filtrates was mixed with double spike solution (DS, ^{111}Cd-^{113}Cd) with a Cd mass DS : sample ratio of 3:2. After a sequence of drying, and digestion, Cd was finally redissolved in 2 mol/L HCl and ready for purification. AG MP-1 M resin was employed for column chemistry, a series HCl different in concentration was used for eluting. Collected eluents were further digested, and finally redissolved in 2% HNO_3 (w/w %) for Cd isotope measurements.

Cadmium isotope composition were analyzed by MC-ICP-MS (Nu Plasma II) with an Aridus II desolvation system. The MC-ICP-MS operating parameters are summarized in Table S2. The Cd isotope composition for all samples were reported as $\delta^{114/110}Cd$ relative to the NIST SRM 3108 standard as:

$$\delta^{114/110}Cd=\left(\frac{^{114/110}Cd_{sample}}{^{114/110}Cd_{standard}}-1\right)\times 1000 \quad (1)$$

The long-term external 2sd (standard deviations) of $\delta^{114/110}Cd$ for each solution were generally better than 0.04‰ for NIST SRM 3108, an in-house reference BGEG-Cd, and Cd stock solution (Figure S3). As isotope composition of sorbed Cd ($\delta^{114/110}Cd_{sorbed}$) may be interfered from residual solution after centrifuging (Barling and Anbar, 2004; Pokrovsky et al., 2014; Yuan et al., 2018), in this work, Cd isotope measurements were performed for all aqueous sample ($\delta^{114/110}Cd_{aqueous}$). And only few $\delta^{114/110}Cd_{sorbed}$ were measured aiming for mass balance confirmation. $\delta^{114/110}Cd_{sorbed}$

were calculated from the measured $\delta^{114/110}Cd_{aqueous}$ and mass balance constraints:

$$\delta^{114/110}Cd_{sorbed}=(\delta^{114/110}Cd_{initial}-f_{aqueous}\times\delta^{114/110}Cd_{aqueous})/(1-f_{aqueous})$$

$$(Error\delta^{114/110}Cd_{sorbed})^2/(\delta^{114/110}Cd_{sorbed})^2=(Error\delta^{114/110}Cd_{aqueous})^2/(\delta^{114/110}Cd_{aqueous})^2 \quad (2)$$

where $f_{aqueous}$ was the fraction of remaining aqueous Cd, and $\delta^{114/110}Cd_{initial}$ refers to the isotope ratios of the Cd stock solution. The associated uncertainties were determined by error propagation with the uncertainties of corresponding $\delta^{114/110}Cd_{aqueous}$ taken into account. Accordingly, the isotopic fractionation of Cd ($\Delta^{114/110}Cd_{aqueous-sorbed}$) between aqueous phase and solid is defined as:

$$\Delta^{114/110}Cd_{aqueous-sorbed} = \delta^{114/110}Cd_{aqueous} - \delta^{114/110}Cd_{sorbed}$$

$$(Error\Delta^{114/110}Cd_{aqueous-sorbed})^2=(Error\delta^{114/110}Cd_{aqueous})^2+(Error\delta^{114/110}Cd_{sorbed})^2 \quad (3)$$

For the experimental data collected in this work, two widely used fractionation models, Equilibrium (eq(4)) and Rayleigh (eq(5)), were used for constraining fractionation factors ($\alpha_{sorbed-aqueous}$) and determining whether the observed fractionations are controlled thermodynamically or kinetically. The two models are described as:

$$\delta^{114/110}Cd_{aqueous}=\frac{\delta^{114/110}Cd_{initial}-1000\times(1-f_{aqueous})\times(\alpha_{sorbed-aqueous}-1)}{f_{aqueous}+(1-f_{aqueous})\times\alpha_{sorbed-aqueous}} \quad (4)$$

$$\delta^{114/110}Cd_{aqueous}=(\delta^{114/110}Cd_{initial}+1000)\times f_{aqueous}^{(\alpha_{sorbed-aqueous}-1)}-1000 \quad (5)$$

Assuming Cd adsorption and desorption reactions are readily reversible, sorbed Cd could sufficiently exchange with aqueous Cd regardless of Cd adsorption fraction at any time, such that the fractionation is thermodynamically driven and would result in two parallel, linear trends (equilibrium fractionation, closed system). In contrast, if

adsorption separates Cd between the aqueous and solid phase, i.e., the adsorption rate is far quicker than desorption or pure kinetic effects, Rayleigh curves are then expected (equilibrium fractionation, open system, or kinetic fractionation) (Wasylenki et al., 2020).

Constrained $\alpha_{sorbed\text{-}aqueous}$ could be used for estimating isotope fractionation ('$\Delta^{114/110}Cd_{aqueous\text{-}sorbed}$, to avoid confusion with equation (3), a superscript is used here) according to:

$$'\Delta^{114/110}Cd_{aqueous\text{-}sorbed} \approx -1000\times\ln(\alpha_{sorbed\text{-}aqueous}) \quad (6)$$

2.4 Mass balance

In order to affirm the validity of our experimental results, the isotope mass balance was calculated for experiments in which both aqueous and relevant sorbed Cd isotope compositions were measured. As per equation (2), the measured $\delta^{114/110}Cd_{aqueous}$ is multiplied by the fraction of Cd remaining dissolved. This value is then added to the product of $\delta^{114/110}Cd_{sorbed}$ and f_{sorbed}, to give a calculated value ($\delta^{114/110}Cd_{m\text{-}b}$) and compared to the $\delta^{114/110}Cd$ values of Cd stock solution ($\delta^{114/110}Cd$ = +0.01±0.04‰). In most cases, the offset between $\delta^{114/110}Cd_{stock}$ and $\delta^{114/110}Cd_{m\text{-}b}$ was smaller than the analytical uncertainty (2sd = 0.04‰) (Table 1 and S3). Despite relatively large scatter in some datasets (e.g., those f_{sorbed} < 20% in MQ water), the mass balance verification lends confidence that our results properly describe the Cd isotope behaviour in this study.

2.5 X-ray absorption spectroscopy measurements and analysis.

Cd K-edge X-ray absorption spectroscopy (XAS) was carried out on beamline 20-BM at the Advanced Photon Source (APS), Argonne, USA. The solid phases separated after centrifuging and freeze-drying were loaded on sample cells and sealed with Kapton tape (Liu et al., 2018; Ye et al., 2022). Four samples were characterized, collected from Cd/$CaCO_3$ ratio experiments with Cd adsorption in MQ water, PO_4^{3-}, -thiol and citrate matrix, respectively. Spectra were collected in fluorescence mode, and the scanning energy range for Cd K-edge was set as 26500-27400 eV. XAS data was initially processed by the Athena program, and subsequently EXAFS by Artemis (Ravel and Newville, 2005; Zhou et al., 2022). All spectra were aligned with the simultaneous measured reference Cd foil with known E^0 of 26711 eV. A linear function was subtracted from the pre-edge region, then the edge jump was normalized using Athena. The $\chi(k)$ data were isolated by subtracting a smooth, two-term polynomial approximating the absorption background. The amplitude reduction factors (S_0^2) were fixed according to the fitting of reference material. The theoretical scattering paths of crystal structures in reference materials were obtained from Cambridge Crystallographic Data Centre database. The evaluation of the fitted coordination number (CN), interatomic distance (R), Debye-Waller factor (σ^2), energy difference (ΔE_0), and goodness of fit (R-factor) were according to Zhou *et al*. (2022).

3. Results

Measured Cd isotope fractionation observed during adsorption in MQ water is

283 shown in Figure 1 and 2 while Figure 3 and 4 show the effects of added (in)organics.
284 All experimental data are tabulated in Tables 1 - 3. Isotope data are presented along
285 with lines predicted by Rayleigh and Equilibrium models (Figure 5 and Table 4). Cd
286 species were studied by Visual MINTEQ 3.1 simulation software (aqueous Cd, Figure
287 S2) and XAS (sorbed Cd, Figure 6), which is setup for Cd isotope fractionation
288 interpretation.
289
290 **3.1 Cd/$CaCO_3$ ratio dependence**
291 For Cd sorbed onto calcite in MQ water, the f_{sorbed} is seen to increase almost
292 linearly from ~20% to 90% (R^2> 0.90, not shown) as calcite loading increases from
293 0.1 to 20 g/L (Figure 1A). Measured $\delta^{114/110}Cd$ also changes in a linear manner with
294 calcite loading, with lighter isotopes preferentially sorbed onto calcite, resulting in
295 heavier $\delta^{114/110}Cd$ values in the remaining aqueous components relative to the initial
296 Cd stock solution (Figure 1B). The degree of Cd isotope fractionation between the
297 aqueous and sorbed phase ($\Delta^{114/110}Cd_{aqueous\text{-}sorbed}$) varied from +0.54‰ to +0.73‰ with
298 average $\Delta^{114/110}Cd_{aqueous\text{-}sorbed}$ = +0.65±0.14‰, which is seen to not vary significantly.

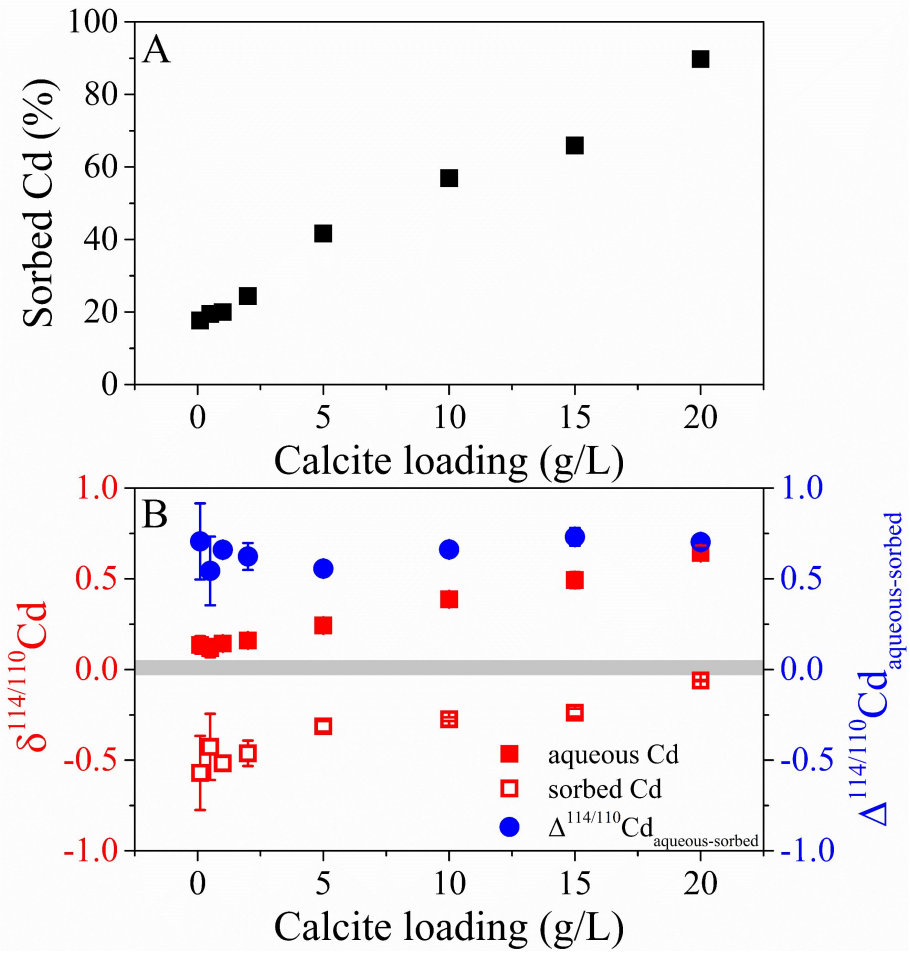

Figure 1. (A) Adsorption of Cd onto calcite in Cd/$CaCO_3$ ratio dependent series, and (B) corresponding Cd isotope composition of the sorbed and remained aqueous Cd as a function of calcite loading in MQ water. The grey area represents the $\delta^{114/110}$Cd of Cd stock solution. Red square marks refer to measured $\delta^{114/110}Cd_{aqueous}$ (■) and corresponding calculated $\delta^{114/110}Cd_{sorbed}$ (□), and blue circles (●) represent isotope fractionation between aqueous and sorbed Cd.

3.2 pH dependence

The behaviour of sorbed Cd observed as pH varied from 5.74 to 8.30 is shown in Figure 2A, with total sorbed Cd increasing which agrees with previous studies (Zachara et al., 1991). While adsorption may generally favorably remove lighter Cd

isotopes from solution (Figure 2B), as pH increases, $\Delta^{114/110}Cd_{aqueous\text{-}sorbed}$ remains constant (Figure 2B) with the average $\Delta^{114/110}Cd_{aqueous\text{-}sorbed}$ of +0.62±0.04‰, indicating Cd isotope fractionation is unaffected by pH variation in the studied range.

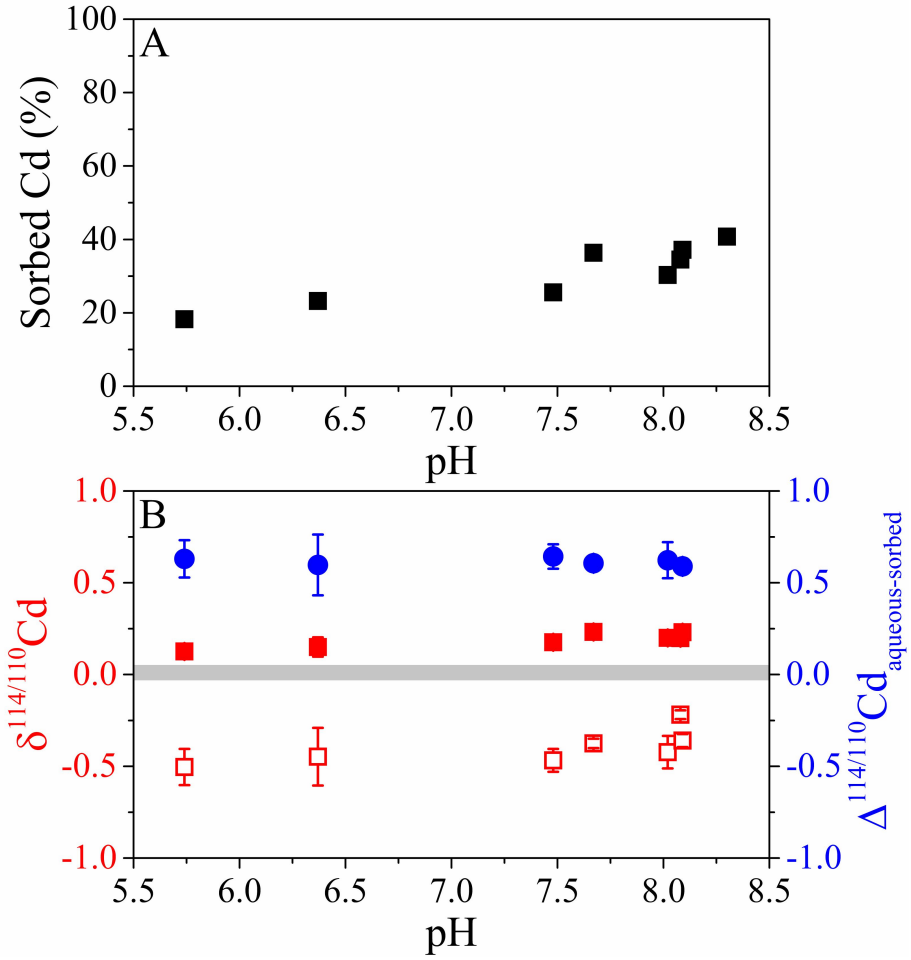

Figure 2. (A) Adsorption of Cd onto calcite in pH dependent series, and (B) corresponding Cd isotope signatures as the function of pH in MQ water. The grey area represents the $\delta^{114/110}Cd$ of Cd stock solution. Squares refer to measured $\delta^{114/110}Cd_{aqueous}$ (■) and corresponding calculated $\delta^{114/110}Cd_{sorbed}$ (□) and blue circles (●) represent isotope fractionation between aqueous and sorbed Cd ($\Delta^{114/110}Cd_{aqueous\text{-}sorbed}$).

3.3 Effects of co-existing (in)organics

The presence of (in)organics are seen to affect Cd adsorption and isotope fractionation. Comparing with Cd adsorption in MQ water, the presence of PO_4^{3-} acted to increase adsorption, while citrate operated to reduce, and -thiol showed no effect on the percentage of adsorbed Cd, respectively (Figure S4). All isotopic results showed that where isotope fractionation occurred adsorption favorably removed lighter Cd isotopes from solution in studied conditions (Figure 3). The average $\Delta^{114/110}Cd_{aqueous\text{-}sorbed}$ of +0.65±0.14‰ obtained in MQ water (Cd/calcite ratio dependence) was slightly raised to +0.69±0.29‰ in the presence of -thiol, and decreased to +0.16±0.15‰ and +0.39±0.12‰ in the presence of PO_4^{3-} and citrate, respectively. In addition, the Cd isotope fractionation with varying pH (pH-dependent experiments) in the presence of these (in)organics was also investigated and similar trends were observed, where the average $\Delta^{114/110}Cd_{aqueous\text{-}sorbed}$ of +0.62±0.04‰ in MQ water was altered to +0.14±0.11‰, +0.61±0.24‰, and +0.38±0.11‰ in the presence of PO_4^{3-}, -thiol and citrate, respectively. Noting that $\Delta^{114/110}Cd_{aqueous\text{-}sorbed}$ in Cd/$CaCO_3$ ratio settings is similar with those in pH dependence.

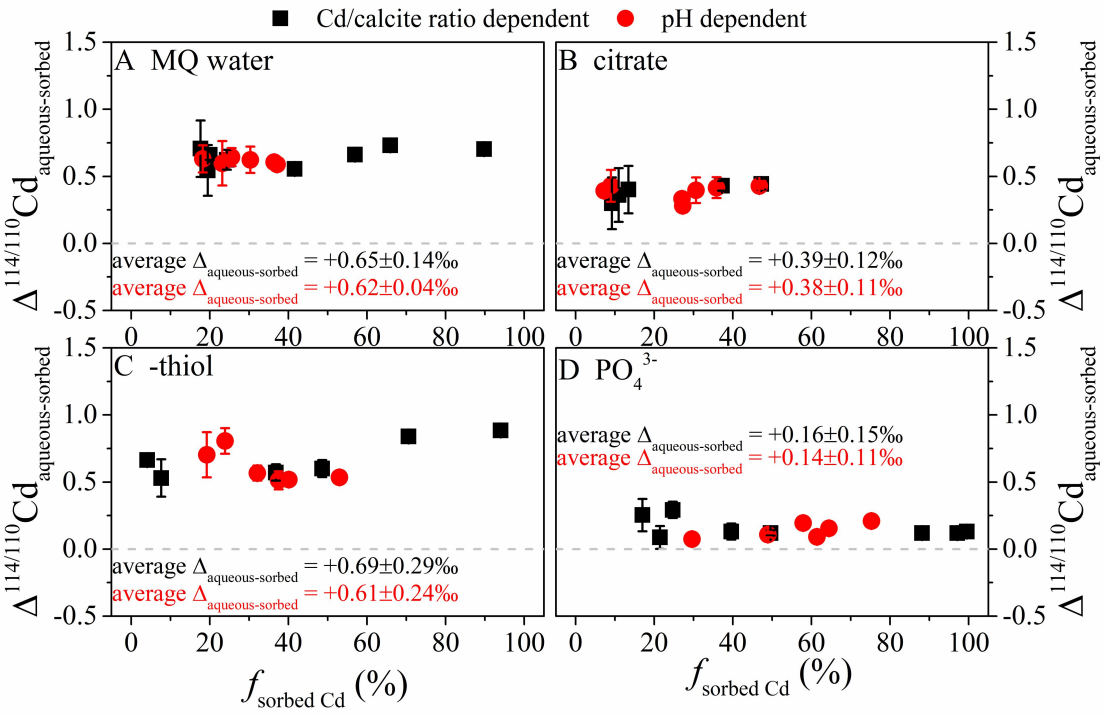

Figure 3. The extent of Cd isotope fractionation ($\Delta^{114/110}Cd_{aqueous-sorbed}$) during Cd adsorption onto calcite as the function of the Cd sorbed fraction in (A) MQ water, (B) citrate, (C) -thiol, and (D) phosphate solution, respectively. Concentration of co-existing (in)organic compounds was 0.1 mmol/L.

For adsorption in the presence of PO_4^{3-}, we further studied the effect of Cd/PO_4^{3-} ratio on Cd isotope fractionation with which varied from 0.25:0.1 to 0.001:0.1 (mmol/L : mmol/L). Results showed that f_{sorbed} rose from ~50% to ~100% with initial Cd decreasing from 0.25 to 0.001 mmol/L, and as the Cd/PO_4^{3-} ratio decreased, measured $\delta^{114/110}Cd_{aqueous}$ changed from +0.05‰ to +0.12‰ which is close to initial Cd stock solution (Figure 4).

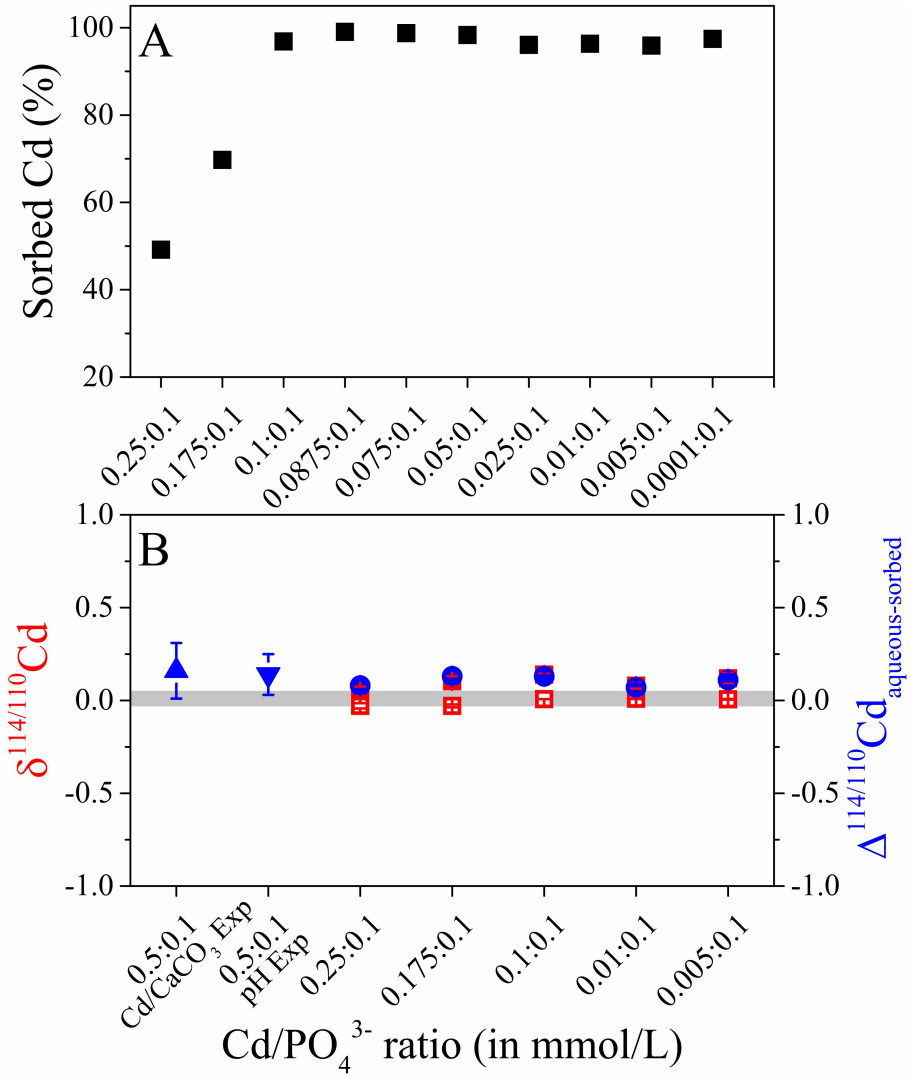

Figure 4. The effect of Cd/PO_4^{3-} ratio on the adsorption of Cd onto calcite (1g/L) (A) and relevant Cd isotope composition of the sorbed and remained aqueous Cd (B). The grey area represents the $\delta^{114/110}Cd$ of Cd stock solution. Squares refer to measured $\delta^{114/110}Cd_{aqueous}$ (■) and corresponding calculated $\delta^{114/110}Cd_{sorbed}$ (□) and blue circles (●) represent isotope fractionation between aqueous and sorbed Cd. Blue triangles, ▲ and ▼, refer to average $\Delta^{114/110}Cd_{aqueous\text{-}sorbed}$ calculated from all data in batch experiments of Cd/calcite ratio and pH dependent (in Figure 3D), respectively.

3.4 Constraint of Cd isotope fractionation factor.

To evaluate Cd isotope fractionation more clearly, all collected and calculated $\delta^{114/110}Cd$ in different batch and preliminary/replicated (Table 1 - 3 and S3) experiments were plotted against the fraction of sorbed Cd for each matrix and consistent Cd isotope behaviour during adsorption in the same matrix was observed clearly (Figure 5). Accordingly, $\alpha_{sorbed\text{-}aqueous}$ was the regressed with best equilibrium fits and Rayleigh curves.

As illustrated in Figure 5A and 5B, the Equilibrium fractionation fitting is visually better than Rayleigh model. Regressions yield $\alpha_{sorbed\text{-}aqueous}$ of 0.99934 (MQ water) and 0.99984 (PO_4^{3-}), respectively (Table 4). The calculated $'\Delta^{114/110}Cd_{aqueous\text{-}sorbed}$ of +0.66‰ (MQ water) and +0.16‰ (PO_4^{3-}) is consistent with the averaged $\Delta^{114/110}Cd_{aqueous\text{-}sorbed}$ of +0.63±0.14‰ (MQ water) and +0.18±0.19‰ (PO_4^{3-}), respectively. However, in Figure 5C and 5D, assessment of which fractionation model fits better is challenging. Equilibrium fractionation yielded $'\Delta^{114/110}Cd_{aqueous\text{-}sorbed}$ of +0.74‰ ($\alpha_{sorbed\text{-}aqueous}$ = 0.99926, -thiol) and +0.40‰ ($\alpha_{sorbed\text{-}aqueous}$ = 0.99960, citrate), respectively (Table 4), which agree well with the average $\Delta^{114/110}Cd_{aqueous\text{-}remained}$ of +0.69±0.26‰ (-thiol) and +0.39±0.13‰ (citrate). The best-fit Rayleigh fractionation regressed $\alpha_{sorbed\text{-}aqueous}$ of 0.99965 (-thiol) and 0.99968 (citrate), respectively. The sum of squared residuals for Equilibrium fitting, 0.403 (-thiol, R^2 = 0.90) and 0.044 (citrate, R^2 = 0.94), seems better over those of 0.481 (-thiol, R^2 = 0.90) and 0.074 (citrate, R^2 = 0.95) for Rayleigh fitting. Using this comparison (Wasylenki et al., 2020), the Equilibrium model shows slightly better goodness-of-fit over the Rayleigh model. From our work we suggest the observed

isotope fractionation during adsorption is thermodynamically driven. The extent of Cd isotope fractionation between sorbed and aqueous decreases in the order of -thiol > MQ water > citrate > PO_4^{3-}. Notably, the presence of PO_4^{3-} significantly decreased Cd isotope fractionation.

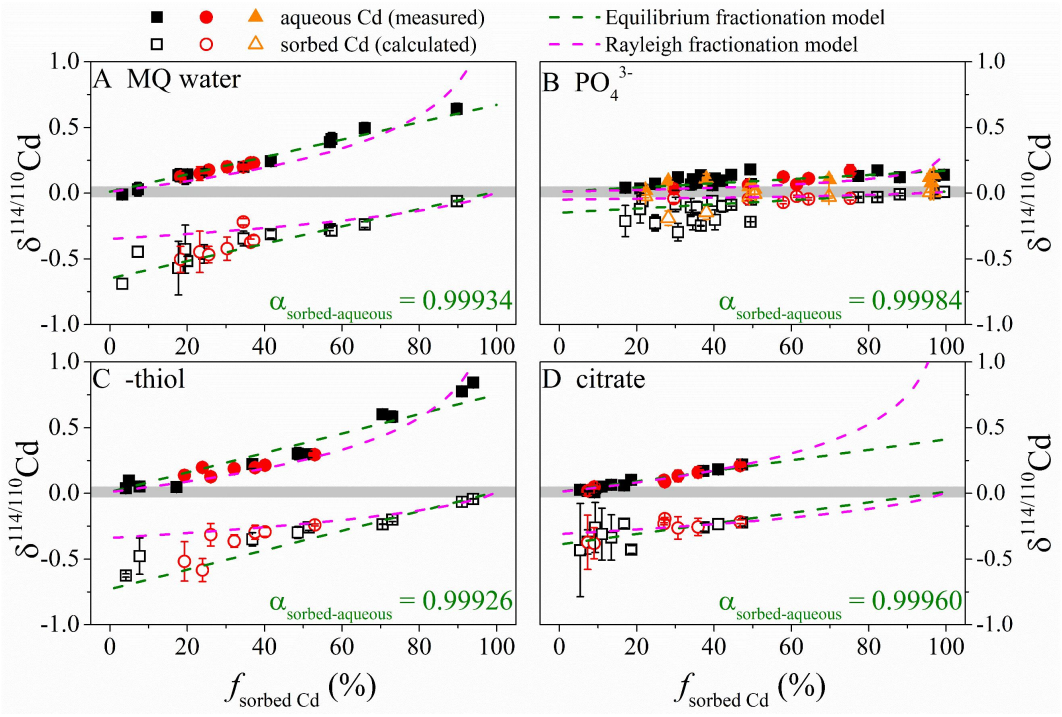

Figure 5. Cd isotope data from all batch, preliminary, and duplicate experiments of the three series settings plotted against the fraction of sorbed Cd. (A), (B), (C), and (D) illustrates the adsorption occurred in MQ water, PO_4^{3-}, -thiol, and citrate solution, respectively. Concentration of co-existing (in)organic compounds was 0.1 mmol/L. The grey area represents the $\delta^{114/110}$Cd of Cd stock solution. Squares (■ and □), circles (● and ○) and triangles (▲ and △) refer to data collected from Cd/$CaCO_3$ ratio dependent, pH dependent and Cd/PO_4^{3-} ratio dependent series. The best-fit isotopic evolution of the residual aqueous and the sorbed Cd are shown with the Equilibrium (---) and Rayleigh (---) fractionation curves. The inserted α were regressed from

Equilibrium fractionation model.

396 Table 1. Isotopic results for batch experiments of Cd adsorption onto calcite in $Cd/CaCO_3$ ratio dependent series.

	$Cd/CaCO_3$ ratio (mmol/L : g/L)	f_{sorbed}	Aqueous		Sorbed				Fractionation		Mass balance
			$\delta^{114/110}Cd$ measured	2sd	$\delta^{114/110}Cd$ calculated	2sd	$\delta^{114/110}Cd$ measured	2sd	$\Delta^{114/110}Cd$ aqueous-sorbed	2sd	$\delta^{114/110}Cd_{m-b}$
MQ water	0.5:0.1	17.7	0.14	0.05	-0.57	0.20	-0.37	0.01	0.71	0.21	0.05
	0.5:0.5	19.5	0.12	0.05	-0.43	0.18	-0.35	0.02	0.54	0.19	0.03
	0.5:1.0	20.0	0.14	0.01	-0.52	0.04	-0.33	0.04	0.66	0.04	0.05
	0.5:2.0	24.4	0.16	0.02	-0.46	0.06	-0.40	0.02	0.62	0.06	0.02
	0.5:5.0	41.6	0.24	0.02	-0.31	0.03	-0.34	0.04	0.56	0.03	0.00
	0.5:10	56.9	0.39	0.01	-0.27	0.01	-0.23	0.03	0.66	0.01	0.04
	0.5:15	65.9	0.49	0.04	-0.24	0.02	-0.25	0.05	0.73	0.04	0.00
	0.5:20	89.8	0.64	0.04	-0.06	0.00	-0.04	0.00	0.70	0.04	0.03
PO_4^{3-}	0.5:0.1	17.0	0.04	0.02	-0.21	0.11			0.25	0.11	
	0.5:0.5	21.5	0.03	0.03	-0.06	0.06	-0.07	0.01	0.09	0.07	0.01
	0.5:1.0	24.8	0.07	0.02	-0.22	0.06			0.29	0.07	
	0.5:2.0	39.6	0.06	0.04	-0.06	0.04			0.13	0.06	
	0.5:5.0	49.6	0.07	0.02	-0.05	0.01			0.12	0.02	
	0.5:10	88.1	0.12	0.03	-0.01	0.01			0.12	0.03	
	0.5:15	97.1	0.13	0.03	0.00	0.01			0.12	0.03	
	0.5:20	99.5	0.14	0.04	0.01	0.00			0.13	0.04	
-thiol	0.5:0.1	4.1	0.04	0.00	-0.63	0.01			0.66	0.00	
	0.5:0.5	7.7	0.05	0.01	-0.48	0.10			0.53	0.10	
	0.5:5.0	36.9	0.22	0.03	-0.35	0.05			0.57	0.06	
	0.5:10	48.6	0.30	0.05	-0.30	0.05	-0.26	0.05	0.60	0.07	0.03

	0.5:15	70.5	0.60	0.00	-0.24	0.00	-0.22	0.04	0.84	0.00	0.02
	0.5:20	94.0	0.84	0.00	-0.04	0.00	-0.10	0.00	0.89	0.00	-0.04
	0.5:0.1	9.3	0.04	0.03	-0.26	0.20			0.30	0.20	
	0.5:0.5	7.3	0.02	0.01	-0.37	0.19					
citrate	0.5:2.0	13.5	0.06	0.03	-0.34	0.17			0.40	0.17	
	0.5:5.0	11.0	0.05	0.03	-0.31	0.19			0.36	0.19	
	0.5:15	37.3	0.17	0.02	-0.26	0.03			0.43	0.04	
	0.5:20	47.3	0.22	0.03	-0.22	0.03			0.44	0.04	

397 $\Delta^{114/110}Cd_{aqueous\text{-}sorbed}$ was calculated using $\delta^{114/110}Cd_{aqueous}$ and $\delta^{114/110}Cd_{sorbed,\ calculated}$

398 $\delta^{114/110}Cd$ for Cd stock solution is +0.01±0.04‰.

399 Table 2. Isotopic results of Cd adsorption experiments in pH dependent series

	pH	f_{sorbed}	Aqueous		Sorbed		Fractionation	
			$\delta^{114/110}$Cd	2sd	$\delta^{114/110}$Cd	2sd	$\Delta^{114/110}$Cd	2sd
			measured		calculated		aqueous-sorbed	
MQ water	5.74	18.2	0.13	0.02	-0.50	0.08	0.63	0.08
	6.37	23.2	0.15	0.05	-0.45	0.15	0.60	0.16
	7.48	25.6	0.18	0.02	-0.47	0.05	0.64	0.06
	7.67	36.4	0.23	0.02	-0.37	0.03	0.61	0.04
	8.02	30.3	0.20	0.04	-0.42	0.08	0.62	0.09
	8.09	37.2	0.23	0.02	-0.36	0.03	0.59	0.04
	8.08	34.5	0.20	0.02	-0.22	0.02		
PO_4^{3-}	5.74	29.6	0.03	0.02	-0.04	0.03	0.07	0.03
	7.48	48.9	0.06	0.02	-0.04	0.01	0.11	0.02
	7.67	61.4	0.07	0.02	-0.02	0.01	0.09	0.02
	8.09	64.5	0.11	0.03	-0.04	0.01	0.15	0.03
	8.30	75.3	0.17	0.05	-0.04	0.01	0.21	0.05
	8.08	57.9	0.12	0.02	-0.07	0.01	0.19	0.02
-thiol	5.74	19.3	0.14	0.04	-0.57	0.16	0.70	0.17
	6.37	23.9	0.20	0.03	-0.61	0.09	0.81	0.10
	7.48	26.1	0.13	0.03	-0.36	0.08		
	7.67	37.5	0.20	0.04	-0.32	0.06	0.51	0.08
	8.02	32.1	0.19	0.03	-0.38	0.06	0.57	0.07
	8.09	40.1	0.21	0.02	-0.30	0.03	0.52	0.03
	8.30	53.0	0.29	0.01	-0.24	0.01	0.54	0.01
citrate	5.74	7.3	0.02	0.04	-0.37		0.39	0.04
	6.37	9.0	0.05	0.02	-0.38	0.15	0.43	0.15
	7.48	27.3	0.09	0.00	-0.19	0.00	0.28	0.00
	7.67	35.9	0.16	0.04	-0.26	0.07	0.42	0.08
	8.02	27.1	0.10	0.00	-0.23	0.00	0.33	0.00
	8.30	46.8	0.21	0.01	-0.22	0.01	0.43	0.01
	8.08	30.7	0.13	0.04	-0.26	0.08	0.40	0.09

400

401 Table 3. Isotopic results of Cd adsorption experiments in Cd/PO_4^{3-} ratio (mmol/L : mmol/L) dependent series

Cd/PO_4^{3-} ratio	f_{sorbed}	Aqueous		Sorbed		Fractionation	
		$\delta^{114/110}Cd$ measured	2sd	$\delta^{114/110}Cd$ calculated	2sd	$\Delta^{114/110}Cd$ aqueous-sorbed	2sd
0.25 : 0.1	49.2	0.05	0.02	-0.03	0.01	0.08	0.03
0.175 : 0.1	69.7	0.10	0.03	-0.03	0.01	0.13	0.03
0.1 : 0.1	96.8	0.14	0.00	0.01	0.00	0.13	0.00
0.01 : 0.1	96.3	0.08	0.02	0.01	0.00	0.07	0.02
0.005 : 0.1	95.9	0.12	0.03	0.01	0.00	0.11	0.03

402

403 Table 4. Fitted $\alpha_{sorbed\text{-}aqueous}$ (Equilibrium fractionation model) for Cd isotope fractionated during Cd adsorption onto calcite in various

404 experiments.

Experiments	$\alpha_{sorbed\text{-}aqueous}$			
	α (all)[a]	α ($Cd/CaCO_3$ ratio-dependence)	α (pH-dependence)	α (Cd/PO_4^{3-} ratio-dependence)
Cd + $CaCO_3$ in MQ	0.99934±0.00002	0.99932±0.00002	0.99940±0.00001	
Cd + $CaCO_3$ + PO_4^{3-}	0.99984±0.00001	0.99983±0.00002	0.99984±0.00002	0.99989±0.00002
Cd + $CaCO_3$ + -thiol	0.99926±0.00004	0.99921±0.00004	0.99946±0.00003	
Cd + $CaCO_3$ + citrate	0.99960±0.00002	0.99958±0.00002	0.99961±0.00002	

405 [a] α (all) represents $\alpha_{sorbed\text{-}aqueous}$ that regressed from all isotope data that in the same matrix.

406 **3.5 Modeled behaviour of Cd species and sorbed Cd coordination geometry.**

407 Results obtained from modeling Cd in solution are presented in Figure S2. In
408 MQ water, $Cd(H_2O)_6^{2+}$ is the predominant species in the studied range (> 97.5%). In
409 the presence of citrate or PO_4^{3-}, $Cd(H_2O)_6^{2+}$ also is the dominant Cd species but at
410 higher pH the fraction is reduced as the proportion of Cd-citrate$^-$ (to ~20%) or
411 Cd-phosphate ($CdHPO_4$, to ~12%) increases.

412 EXAFS analysis of experimental materials, undertaken to obtain information
413 about oxidation states and chemical bonding is detailed in Figure 6 and Table S4. All
414 four EXAFS patterns showed first-shell peaks at ~2.28 Å, which agrees well with
415 reported Cd-O bond length at the first-shell (Fulda et al., 2013; Sun et al., 2019b), and
416 second-shell peaks at ~3.15 Å accords with Cd-C (~3.14 Å) in $CdCO_3$ crystal (Fulda
417 et al., 2013). Combining the rational fits using $CdCO_3$ crystal as structural model
418 (Figure 6) and unreasonable results using paths in $Cd(OH)_2$, CdS, $Cd_3(PO_4)_2$ (not
419 shown), we considered $CdCO_3$ crystal is the best-fit reference and regarded the
420 formation of Cd inner-sphere complexes on the calcite surface. The fitted bond length
421 of 2.27-2.29 Å (Cd-O) and 3.12-3.15 Å (Cd-C) for sorbed Cd species is close to
422 previous reported values (Fulda et al., 2013; Sun et al., 2019b). Regarding
423 coordination number (CN), in the first-shell, sorbed Cd with PO_4^{3-} seems to be
424 coordinated with fewer O atoms than in other three samples, indicated by lower Cd-O
425 signal (first shell) of sorbed Cd (PO_4^{3-}) (Figure S5). For MQ water, -thiol, and citrate,
426 sorbed Cd was surrounded by 7.0, 6.8, and 7.2 O atoms, respectively, all of which are
427 greater than the value previously reported for aqueous Cd (CN = 6, MQ water (Sun et

al., 2019b)). Noting that with PO_4^{3-}, sorbed Cd was surrounded by 5.9 O atoms, appearing to be in close agreement aqueous Cd reported by Sun *et al.* (2019b) (CN = 6, MQ water).

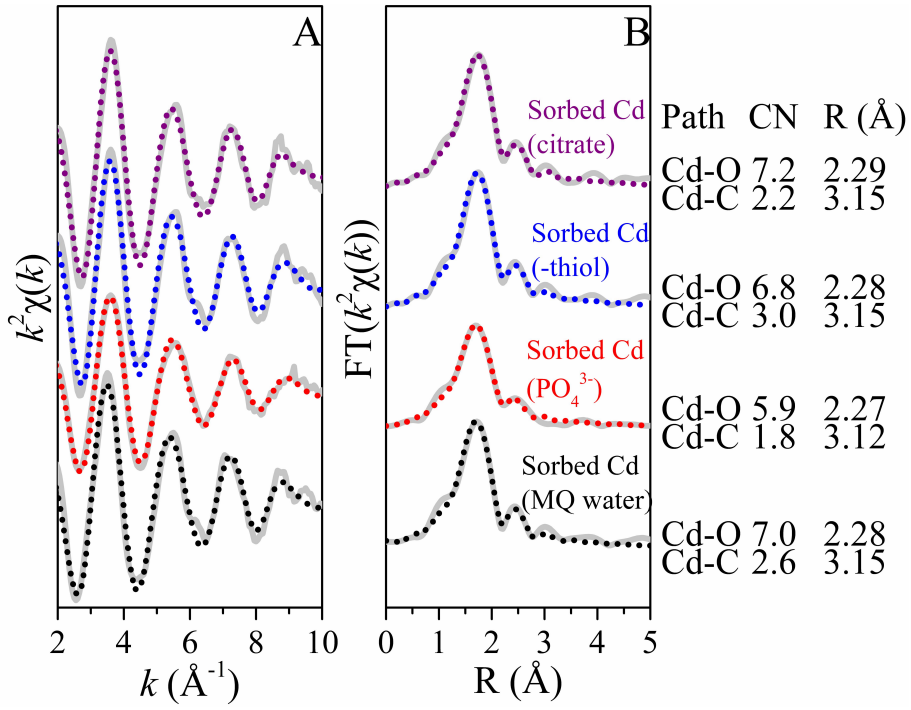

Figure 6. Cd *K*-edge XAS spectra (A for raw k^2 weighted functions and B for Fourier-transform magnitudes without shift correction) of centrifugated solid phase from adsorption experiments under various conditions (in Cd/$CaCO_3$ ratio dependent experiments, calcite loading: 20 g/L). Raw data are shown as gray solid lines, and fitted data are shown as colored dash lines. Fitting results are also summarized in Table S4.

In summary, with all solutions used in this study, lighter isotopes are preferentially adsorbed with isotope ratios in the solution being heavier than in the adsorbed species. $\Delta^{114/110}Cd_{aqueous\text{-}sorbed}$ is independent of either Cd/calcite ratio, pH or Cd/PO_4^{3-} ratio in the studied range. And for the selected solutions, $\Delta^{114/110}Cd_{aqueous\text{-}sorbed}$

443 is noted to decrease in the order of -thiol > MQ > citrate > PO_4^{3-}. Factors influencing
444 isotope fractionation include target coordination environment, and EXAFS results
445 confirmed coordination geometry for sorbed Cd were somewhat differed from
446 aqueous Cd species.
447
448 **4. Discussion**
449 **4.1 Cadmium – calcite systematics**
450 **4.1.1 Chemical adsorption**
451 Solution chemistry will determine the nature of the adsorbate species and the
452 surface site complexing of the adsorbate species. The mechanisms operating during
453 surface adsorption of divalent cations onto calcite surfaces have been studied
454 extensively using surface complexation models (SCMs) (Alvarez et al., 2020;
455 Pokrovsky et al., 2000; Pokrovsky and Schott, 2002; Yuan et al., 2018). According to
456 the established calcite SCMs, primary hydration sites (such as $>CO_3H^0$) would be
457 protonated/deprotonated successively and then used for capturing aqueous ions. Cd
458 sorbed onto calcite could thus be described as:
459 $$>CO_3^- + Cd^{2+} \rightarrow >CO_3Cd^+ \quad (7)$$
460 where $>CO_3^-$ refers to a deprotonated adsorption site and $>CO_3Cd^+$ represents the
461 corresponding Cd surface species on the site. The adsorption of Cd species in solution
462 by an active surface will be affected by the solution chemistry and the nature of the
463 surface target sites. In particular, the linear increase of sorbed Cd with calcite loading
464 (Figure 1A) reveals that aqueous Cd sorbed onto calcite was a surface-mediated

process, probably limited by available specific surface sites. Changes of solution pH show an increase in adsorbed Cd as pH increases from 5.74 to 8.30 (Figure 2A), which is consistent with previous work (Zachara et al., 1991). According to equation (7), increasing solution pH could enhance deprotonation of primary adsorption sites causing an increase in overall negative surface charge, i.e., increase of $>CO_3^-$ site. The solution chemistry, i.e., pH, is likely to affect the adsorbate species. However, aqueous Cd species changes (dominated as $Cd(H_2O)_6^{2+}$) are negligible in the studied range (Figure S2). Therefore, enhanced adsorption as pH increases may result from the buildup of more negative charges on the surface of the calcite and increased $>CO_3^-$ adsorption site (Zachara et al., 1991).

Insights into the mechanism of Cd adsorption may be gained from Cd isotope ratios, because isotope fractionation is generally highly sensitive to the differences in complexation geometry between aqueous and sorbed speciation. For example, the alteration of W species during W adsorption onto birnessite were captured by W isotope signatures (Wasylenki et al., 2020). In this work, the $\delta^{114/110}Cd$ collected in the same matrix are comparable and could be described by one Equilibrium model trend (Figure 5). This result suggests the formation of the same type of inner-sphere Cd complex on calcite in the same matrix, and the formed Cd surficial species is independent of Cd/calcite ratio, pH and Cd/PO_4^{3-} ratio in the studied range (Wasylenki et al., 2020; Yan et al., 2021). This idea is supported by EXAFS results showing the same coordination environments for sorbed Cd and Cd sorbed onto iron (oxyhydr)oxides (Yan et al., 2021) and δ-MnO_2 (Sun et al., 2019a) under various

surface loading and pH conditions. However, compared to $'\Delta^{114/110}Cd_{aqueous\text{-}sorbed}$ of +0.66‰ in MQ water, the presence of (in)organics alters $'\Delta^{114/110}Cd_{aqueous\text{-}sorbed}$ to +0.16‰ (PO_4^{3-}), +0.74‰ (-thiol), and +0.40‰ (citrate), respectively. This result indicates the change of coordination geometry from aqueous to surficial Cd species are different in the four studied matrixes.

Thus, Cd sorbed on to calcite is a surface site limited process and deprotonation of $>CO_3H^0$ leads to enhanced Cd adsorption as pH increases. Cd isotope signatures indicate the sorbed Cd species in the same matrix are in the same type in the studied range.

4.1.2 Cd isotope fractionation

$\Delta^{114/110}Cd_{aqueous\text{-}sorbed}$ is controlled by isotope adsorption kinetics and isotope exchange between sorbed and aqueous species. As mentioned above, the comparable Cd isotope fractionation in the same chemical matrix (Figure 3) suggests the observed isotope behaviour is controlled by the same mechanism. In this work, Cd isotopes were observed to fractionate with light isotopes being preferentially adsorbed, and the fractionation is thermodynamically driven equilibrium fractionation (Figure 5). Therefore, the relative abundance of Cd isotopes in sorbed and aqueous species is determined by the differences in coordination environments of the two phases. No Cd oxidation state alteration is expected during adsorption. Here we speculate that the observed Cd isotope fractionation, lighter isotopes enriched in sorbed species, is triggered by changes in Cd coordination geometry after adsorption.

For equilibrium isotope fractionation, heavier isotopes preferably enriched in stronger coordination environments, including lower coordination number (CN), shorter bond length and stronger bond stiffness between central and neighbor atoms (Wiederhold, 2015). For example, the observed $\Delta^{114/110}Cd_{aqueous\text{-}sorbed}$ of +0.24‰ at low ionic strength during adsorption by birnessite is presumed to be because the Cd-O bond length in the highly distorted sorbed Cd (Cd-O_6) would be ~0.08 Å longer than hydrated Cd ions (Wasylenki et al., 2014). And Yan *et al*. (2021) ascribed lighter Cd in sorbed phases to highly distorted of sorbed Cd (Cd-O_6) compared to aqueous Cd based on EXAFS results.

Previous works showed Cd-O length of 2.27 Å for hydrated $Cd(H_2O)_6^{2-}$ species (Sun et al., 2019b), although we did not have EXAFS data of aqueous Cd in the other three matrixes, we suspect there will be negligible changes from 2.27 Å since $Cd(H_2O)_6^{2+}$ is the dominant species in all case (> 80%). Our EXAFS data shows slightly longer (~0.02 Å) of Cd-O in sorbed rather than aqueous Cd species (Figure 6 and Table S4), suggesting the distortion of octahedral Cd-O_6, which agrees with other studies about Cd sorbed onto various mineral substrates (Spadini et al., 1994; Sun et al., 2018; Sun et al., 2019b; Vasconcelos et al., 2008). Coordination number (CN) in the first shell for sorbed Cd in the cases of MQ water, -thiol, and citrate were greater than that of $Cd(H_2O)_6^{2-}$, whilst close to $Cd(H_2O)_6^{2-}$ in the presence of PO_4^{3-} (Figure 6 and Table S4). Because of the increased CN of O atoms and subtly lengthened Cd-O bond length, octahedral Cd-O_6 would be distorted to a different degree when aqueous Cd sorbed as inner-sphere complex in the cases of MQ water, -thiol, and citrate,

which could explain the enrichment of isotopically lighter Cd isotope on the calcite surface in light of equilibrium theory (Schauble, 2004; Wiederhold, 2015). In contrast, the Cd coordination environment barely changes in the case of PO_4^{3-}, which may explain the very small Cd isotope fractionation ('$\Delta^{114/110}Cd_{aqueous\text{-}sorbed}$ of +0.16‰).

In our experiments, $\Delta^{114/110}Cd_{aqueous\text{-}sorbed}$ was seen to decrease in the order -thiol > MQ water > citrate > PO_4^{3-}. But the discussion above can only give a qualitative interpretation of favorable adsorption of lighter Cd isotopes, the quantitative explanation of our isotope data, such as why greater Cd isotope fractionation occurs in the presence of -thiol than MQ water, remains unclear. We suspect it is likely related with the complexation effect of organic substances (Ratié et al., 2021; Zhao et al., 2021). In particular, a recent theoretical work revealed that Cd isotope composition in Cd-organic complexes decreases in the order of Cd-citrate complex > $Cd(H_2O)_6^{2+}$ > Cd-thiol species (Zhao et al., 2021). Assuming the presence of (in)organics affected surface Cd species, e.g., calcite-Cd-ligands inner-sphere complex (Boily and Fein, 1996; Shirvani et al., 2006b; Tiberg and Gustafsson, 2016), isotope compositions in sorbed Cd were also expected as Cd-citrate complex > $Cd(H_2O)_6^{2+}$ > Cd-thiol species, which supports the observed decreasing values '$\Delta^{114/110}Cd_{aqueous\text{-}sorbed}$ in the order of -thiol > MQ water > citrate.

4.1.3 Differences in Cd isotope fractionation between co-precipitation and adsorption

A number of studies have investigated isotope fractionation during adsorption

553 onto calcite. For example, the enrichment of lighter Ni (Alvarez et al., 2020) and Ga
554 (Yuan et al., 2018) but heavier Zn (Dong and Wasylenki, 2016) in sorbed fractions
555 were observed with $\Delta^{60}Ni_{aqueous\text{-}sorbed}$ = +0.52‰, $\Delta^{71}Ga_{aqueous\text{-}sorbed}$ = +1.27‰, and
556 $\Delta^{66}Zn_{aqueous\text{-}sorbed}$ = -0.41‰ and -0.73‰, respectively. Our results demonstrate calcite
557 preferably adsorbs light Cd isotopes in the studied conditions ('$\Delta^{114/110}Cd_{aqueous\text{-}sorbed}$ =
558 +0.66‰, in MQ water). This fractionation is similar but greater than
559 $\Delta^{114/110}Cd_{aqueous\text{-}sorbed}$ values during Cd sorbed onto Mn oxyhydroxide (+0.24‰
560 (Wasylenki et al., 2014)) and iron (oxyhydr)oxides (~+0.50‰ (Yan et al., 2021)).
561 Notably, our observation of '$\Delta^{114/110}Cd_{aqueous\text{-}sorbed}$ = +0.66‰ is contrary to the reported
562 absence of Cd isotope fractionation while Cd co-precipitated into calcite in fresh
563 water reported by Horner *et al*. (2011). In addition, Rayleigh fractionation, in contrast
564 to equilibrium fractionation in this work, was observed in artificial seawater
565 ($\alpha_{calcite\text{-}aqueous}$ of 0.99955 (Horner et al., 2011)) and groundwater ($\alpha_{calcite\text{-}aqueous}$ of
566 0.99905 (Xie et al., 2020)) matrix during co-precipitation. These differences between
567 adsorption and co-precipitation might impact the interpretation and application of
568 natural carbonate Cd isotope signals.

569 Adsorption induced isotope fractionation was generally influenced by adsorption
570 conditions including surface loading, pH value *etc*. For example, Gou *et al*. (2018)
571 found no Zn isotope fractionation at pH 7.0-8.0 during Zn sorbed onto γ-Al_2O_3
572 because the formed layered double hydroxide Zn species in this condition featured
573 close Zn binding environment to aqueous Zn. But $\Delta^{66}Zn_{aqueous\text{-}sorbed}$ = -0.47‰ was
574 obtained at pH 6-6.5 since the formation of inner-sphere Zn surficial complex is

575 tetrahedral compare to octahedral aqueous Zn (Gou et al., 2018). However, Yan *et al.*
576 (2021) recently showed Cd isotope fractionation is pH- and surface loading
577 independent when adsorption onto iron (oxyhydr)oxides, which is also consistent with
578 our observation during Cd adsorption on calcite. Both Yan *et al.* (2021) and our study
579 ascribed the isotope fractionation to the formation of the same type of inner-sphere Cd
580 surficial complex.

581 Diverse Cd isotope signatures were obtained during Cd sorbed onto calcite under
582 different matrix conditions, supporting the significance of Cd solution chemistry on
583 Cd isotope behaviour during adsorption. In this work, the extent of Cd isotope
584 fractionation between sorbed and aqueous species decreased in the order of -thiol >
585 MQ water > citrate > PO_4^{3-}. Some recent works also showed $Cd(H_2O)_6^{2+}$ is
586 isotopically lighter than -thiol Cd species but heavier than and -carboxyl Cd
587 compounds (Ratié et al., 2021; Zhao et al., 2021). Notably, we found the presence of
588 PO_4^{3-} decreased $\Delta^{114/110}Cd_{aqueous\text{-}sorbed}$ significantly to a certainly small value (averaged
589 $\Delta^{114/110}Cd_{aqueous\text{-}sorbed}$ of +0.63‰ *vs.* +0.18‰), which could be resolved from other
590 conditions, such as Cd sorbed onto Mn oxyhydroxide (Wasylenki et al., 2014) and
591 iron (oxyhydr)oxides (Yan et al., 2021), and Cd-calcite co-precipitation (Horner et al.,
592 2011; Xie et al., 2020). The distinguishable isotope characteristic may indicate that
593 PO_4^{3-} would be an important factor for natural Cd isotope signatures interpretation.

594

595 **4.2 Geochemical implications**

596 Co-precipitation and adsorption are two important processes operating during Cd

incorporation into carbonates. Our results show that Cd isotopes behave differently in these two processes, observed in different degrees of isotope fractionation. Consequently, Cd isotope signals preserved in carbonates may result from both Cd adsorption and co-precipitation. It is well demonstrated that Cd isotope signals preserved in sedimentary carbonates may serve as a reliable proxy for paleoenvironment applications, such as reconstructing $\delta^{114/110}$Cd of ancient seawater (Zhang et al., 2018). However, it is required to understand the Cd isotope fractionation in the dominant process of interest (Wasylenki et al., 2014). The findings in this work give an alternative consideration in addition to co-precipitation to interpret carbonated Cd isotope signatures (Zhang et al., 2018). On the other hand, metal transfer into calcite by both adsorption and co-precipitation are potentially significant to the global metal budget and associated isotope mass balance (Alvarez et al., 2021; Alvarez et al., 2020). Therefore, correctly determined fractionation factors correlated to important Cd outputs, including co-precipitation into calcite (Horner et al., 2011; Xie et al., 2020), adsorption onto birnessite (Wasylenki et al., 2014) and Fe-(oxyhydr)oxides (Yan et al., 2021), precipitation as CdS (Guinoiseau et al., 2018), uptake by phytoplankton (Horner et al., 2013; Lacan et al., 2006), and adsorption onto calcite (this work), will be beneficial to better clarify the Cd global cycles and relevant isotope mass balance.

Adsorption of metal ions onto calcite is ubiquitous in the environment (Zachara et al., 1991; Zachara et al., 1988). However, their adsorption behaviour may be strongly affected by the local environmental (in)organics such as phosphate, -thiol,

-carboxyl, sulfate, silicate, chloride compounds *etc* (Davis and Leckie, 1978). For example, bidentate inner-sphered Cd complex could be formed during Cd adsorbed onto goethite in the presence of phosphate, sulphate and humate, while Cd could even be precipitated in the presence of citrate and oxalate (Collins et al., 1999). The presence of (in)organics can not only alter the adsorption process, but also influence the preserved isotope signature since isotope fractionation is correlated with species alteration (Wiederhold, 2015). A recent work showed that the formation of Zn−Al layered double hydroxide during Zn sorbed onto γ-Al_2O_3 surface resulted in no Zn isotope fractionation, but the presence of Si (> 0.64 mM) would lead to the formation of inner-sphere ternary >Al−Si−Zn species, and $\Delta^{66}Zn_{aqueous\text{-}sorbed}$ = -0.63‰ was observed (Gou et al., 2018; Gou et al., 2022). This study highlighted the role of co-existing Si for evaluating Zn isotope signals in relevant environments. Our study demonstrates the presence of (in)organics could alter Cd isotope fractionation during adsorption, for example, ' $\Delta^{114/110}Cd_{aqueous\text{-}sorbed}$ = +0.66‰ in MQ water was astonishingly reduced to +0.16‰ in the presence of PO_4^{3-} no matter conditions varied in studied range. Considering Cd and some (in)organics (e.g., PO_4^{3-}) are shown to be coupled during (bio)geochemical cycles and especially, marine Cd shows a nutrient-like distribution that closely correlates with nutrient PO_4^{3-} (Boyle et al., 1976; de Souza et al., 2022; Duhamel et al., 2021). Experimental and theoretical works should carefully consider the effects of PO_4^{3-} and/or other (in)organics on Cd isotope behaviour during Cd uptake into minerals (carbonates, Fe and Mn (oxyhydr)oxides etc.) by both co-precipitation and adsorption.

5. Conclusions

The present study provides constraints on Cd isotope fractionation during adsorption onto calcite. The obtained results offer valuable information on Cd isotope signature interpretation for applying Cd isotopes as tracers in geochemical and environmental investigations. The primary findings could be summarized as follows:

1. Cd adsorption is controlled by solution chemistry, and lighter Cd is preferentially sorbed with $\Delta^{114/110}Cd_{aqueous\text{-}sorbed}$ not influenced by Cd/calcite ratios and pH values in the studied range.

2. Cd isotope fractionation follows equilibrium trends and $'\Delta^{114/110}Cd_{aqueous\text{-}sorbed}$ = +0.66‰ was measured in MQ water. $'\Delta^{114/110}Cd_{aqueous\text{-}sorbed}$ was altered when (in)organic compounds were present during adsorption. $'\Delta^{114/110}Cd_{aqueous\text{-}sorbed}$ was lowered to +0.16‰ in the presence of PO_4^{3-}. This indicates the important role of PO_4^{3-} in Cd isotope signature interpretation as Cd co-occurrence with PO_4^{3-} is expected in seawater, underground water and minerals.

3. Distortion of the octahedral Cd-O_6 constituting the surficial Cd structures could trigger significant preferential adsorption of lighter Cd in matrices of MQ water, -thiol, and citrate, whereas barely changed Cd coordination geometry after adsorption in the presence of PO_4^{3-} could contribute to the observed insignificant fractionation.

4. Adsorption induced Cd isotope fractionation is different from that caused by co-precipitation, the reported fractionation factors provide another potential interpretation associated with Cd in carbonate minerals.

Acknowledgements

This work was financially supported by National Natural Science Foundation of China (21822405, 41673014 and 41521001). The Cd XAS characterization was performed at Beamline Sector 20-BM of the Advanced Photon Source, Argonne National Laboratory.

Appendix A. Supplementary Information

Supplementary Information associated with this article can be found in the online version.

References:

Alvarez, C.C., Quitté, G., Schott, J. and Oelkers, E.H., 2021. Nickel isotope fractionation as a function of carbonate growth rate during Ni coprecipitation with calcite. Geochim. Cosmochim. Acta 299, 184-198. https://doi.org/10.1016/j.gca.2021.02.019

Alvarez, C.C., Schott, J. and Oelkers, E.H., 2020. Experimental determination of Ni isotope fractionation during Ni adsorption from an aqueous fluid onto calcite surfaces. Geochim. Cosmochim. Acta 273, 26-36. https://doi.org/10.1016/j.gca.2020.01.010

Barling, J. and Anbar, A.D., 2004. Molybdenum isotope fractionation during adsorption by manganese oxides. Earth. Planet. Sci. Lett. 217, 315-329.

https://doi.org/10.1016/S0012-821X(03)00608-3

Boily, J.-F. and Fein, J.B., 1996. Experimental study of cadmium-citrate co-adsorption onto α-Al_2O_3. Geochim. Cosmochim. Acta 60, 2929-2938. https://doi.org/10.1016/0016-7037(96)00131-7

Bottcher, M., 1997. Solid solution partitioning of Sr^{2+}, Ba^{2+}, and Cd^{2+} to calcite. Geochim. Cosmochim. Acta 3, 661-662.

Boyle, E.A., Sclater, F. and Edmond, J.M., 1976. On the marine geochemistry of cadmium. Nature 263, 42-44. https://doi.org/10.1038/263042a0

Brown, G.E. and Parks, G.A., 2001. Sorption of trace elements on mineral surfaces: modern perspectives from spectroscopic studies, and comments on sorption in the marine environment. Intl. Geol. Rev. 43, 963-1073. https://doi.org/10.1080/00206810109465060

Collins, C.R., Ragnarsdottir, K.V. and Sherman, D.M., 1999. Effect of inorganic and organic ligands on the mechanism of cadmium sorption to goethite. Geochim. Cosmochim. Acta 63, 2989-3002. https://doi.org/10.1016/S0016-7037(99)00226-4

Comans, R.N.J. and Middelburg, J.J., 1987. Sorption of trace metals on calcite: Applicability of the surface precipitation model. Geochim. Cosmochim. Acta 51, 2587-2591. https://doi.org/10.1016/0016-7037(87)90309-7

Davis, J.A., Fuller, C.C. and Cook, A.D., 1987. A model for trace metal sorption processes at the calcite surface: Adsorption of Cd^{2+} and subsequent solid solution formation. Geochim. Cosmochim. Acta 51, 1477-1490.

https://doi.org/10.1016/0016-7037(87)90330-9

Davis, J.A. and Leckie, J.O., 1978. Effect of adsorbed complexing ligands on trace metal uptake by hydrous oxides. Environ. Sci. Technol. 12, 1309-1315. https://doi.org/10.1021/es60147a006

de Souza, G.F., Vance, D., Sieber, M., Conway, T.M. and Little, S.H., 2022. Re-assessing the influence of particle-hosted sulphide precipitation on the marine cadmium cycle. Geochim. Cosmochim. Acta 322, 274-296. https://doi.org/10.1016/j.gca.2022.02.009

Dong, S. and Wasylenki, L.E., 2016. Zinc isotope fractionation during adsorption to calcite at high and low ionic strength. Chem. Geol. 447, 70-78. https://doi.org/10.1016/j.chemgeo.2016.10.031

Duhamel, S., Diaz, J.M., Adams, J.C., Djaoudi, K., Steck, V. and Waggoner, E.M., 2021. Phosphorus as an integral component of global marine biogeochemistry. Nat. Geosci. 14, 359-368. https://doi.org/10.1038/s41561-021-00755-8

Fujii, T. and Albarède, F., 2012. Ab initio calculation of the Zn isotope effect in phosphates, citrates, and malates and applications to plants and soil. PLoS One 7, e30726. https://doi.org/10.1371/journal.pone.0030726

Fulda, B., Voegelin, A. and Kretzschmar, R., 2013. Redox-controlled changes in cadmium solubility and solid-phase speciation in a paddy soil as affected by reducible sulfate and copper. Environ. Sci. Technol. 47, 12775-12783. https://doi.org/10.1021/es401997d

Georgiev, S.V., Horner, T.J., Stein, H.J., Hannah, J.L., Bingen, B. and Rehkämper, M.,

729 2015. Cadmium-isotopic evidence for increasing primary productivity during
730 the Late Permian anoxic event. Earth. Planet. Sci. Lett. 410, 84-96.
731 http://doi.org/10.1016/j.epsl.2014.11.010
732 Gou, W., Li, W., Ji, J. and Li, W., 2018. Zinc isotope fractionation during sorption
733 onto Al oxide: Atomic level understanding from EXAFS. Environ. Sci.
734 Technol. 52, 9087-9096. https://doi.org/10.1021/acs.est.8b01414
735 Gou, W., Li, W., Siebecker, M.G., Zhu, M., Li, L. and Sparks, D.L., 2022. Coupling
736 molecular-scale spectroscopy with stable isotope analyses to investigate the
737 effect of Si on the mechanisms of Zn–Al LDH formation on Al oxide. Environ.
738 Sci. Technol. 56, 13829-13836. https://doi.org/10.1021/acs.est.2c05140
739 Guinoiseau, D., Galer, S.J.G. and Abouchami, W., 2018. Effect of cadmium sulphide
740 precipitation on the partitioning of Cd isotopes: implications for the oceanic
741 Cd cycle. Earth. Planet. Sci. Lett. 498, 300-308.
742 https://doi.org/10.1016/j.epsl.2018.06.039
743 Hay, M.B., Workman, R.K. and Manne, S., 2003. Mechanisms of metal ion sorption
744 on calcite: Composition mapping by lateral force microscopy. Langmuir 19,
745 3727-3740. https://doi.org/10.1021/la020647s
746 Horner, T.J., Lee, R.B.Y., Henderson, G.M. and Rickaby, R.E.M., 2013. Nonspecific
747 uptake and homeostasis drive the oceanic cadmium cycle. Proc. Nat. Acad. Sci.
748 110, 2500-2505. https://doi.org/10.1073/pnas.1213857110
749 Horner, T.J., Rickaby, R.E.M. and Henderson, G.M., 2011. Isotopic fractionation of
750 cadmium into calcite. Earth. Planet. Sci. Lett. 312, 243-253.

https://doi.org/10.1016/j.epsl.2011.10.004

Kozar, S., Bilinski, H. and Branica, M., 1992. Adsorption of lead and cadmium ions on calcite in the Krka estuary. Mar. Chem. 40, 215-230. https://doi.org/10.1016/0304-4203(92)90024-5

Kubier, A., Wilkin, R.T. and Pichler, T., 2019. Cadmium in soils and groundwater: A review. Appl. Geochem. 108, 104388. https://doi.org/10.1016/j.apgeochem.2019.104388

Lacan, F., Francois, R., Ji, Y. and Sherrell, R.M., 2006. Cadmium isotopic composition in the ocean. Geochim. Cosmochim. Acta 70, 5104-5118. https://doi.org/10.1016/j.gca.2006.07.036

Liu, P., Ptacek, C.J., Elena, K.M.A., Blowes, D.W., Gould, W.D., Finfrock, Y.Z., Wang, A.O. and Landis, R.C., 2018. Evaluation of mercury stabilization mechanisms by sulfurized biochars determined using X-ray absorption spectroscopy. J. Hazard. Mater. 347, 114-122. https://doi.org/10.1016/j.jhazmat.2017.12.051

Martin-Garin, A., Van Cappellen, P. and Charlet, L., 2003. Aqueous cadmium uptake by calcite: A stirred flow-through reactor study. Geochim. Cosmochim. Acta 67, 2763-2774. https://doi.org/10.1016/S0016-7037(03)00091-7

Meyer, K.M. and Kump, L.R., 2008. Oceanic euxinia in earth history: causes and consequences. Ann. Rev. Earth Planet. Sci. 36, 251-288. https://doi.org/10.1146/annurev.earth.36.031207.124256

Morse, J.W., 1986. The surface chemistry of calcium carbonate minerals in natural

773 waters: An overview. Mar. Chem. 20, 91-112.
774 https://doi.org/10.1016/0304-4203(86)90068-X
775 Peng, H., He, D., Guo, R., Liu, X., Belshaw, N.S., Zheng, H., Hu, S. and Zhu, Z.,
776 2021. High precision cadmium isotope analysis of geological reference
777 materials by double spike MC-ICP-MS. J. Anal. At. Spectrom. 36, 390-398.
778 https://doi.org/10.1039/D0JA00424C
779 Pokrovsky, O.S., Galy, A., Schott, J., Pokrovski, G.S. and Mantoura, S., 2014.
780 Germanium isotope fractionation during Ge adsorption on goethite and its
781 coprecipitation with Fe oxy(hydr)oxides. Geochim. Cosmochim. Acta 131,
782 138-149. https://doi.org/10.1016/j.gca.2014.01.023
783 Pokrovsky, O.S., Mielczarski, J.A., Barres, O. and Schott, J., 2000. Surface speciation
784 models of calcite and dolomite/aqueous solution interfaces and their
785 spectroscopic evaluation. Langmuir 16, 2677-2688.
786 https://doi.org/10.1021/la980905e
787 Pokrovsky, O.S. and Schott, J., 2002. Surface chemistry and dissolution kinetics of
788 divalent metal carbonates. Environ. Sci. Technol. 36, 426-432.
789 https://doi.org/10.1021/es010925u
790 Prieto, M., Cubillas, P. and Fernández-Gonzalez, Á., 2003. Uptake of dissolved Cd by
791 biogenic and abiogenic aragonite: A comparison with sorption onto calcite.
792 Geochim. Cosmochim. Acta 67, 3859-3869.
793 https://doi.org/10.1016/S0016-7037(03)00309-0
794 Qin, Z., Li, D. and Liu, S. 2019 Cadmium isotope fractionation during adsorption

onto Kaolinite, AGU fall meeting, pp. V51E-0107.

Ratié, G., Chrastný, V., Guinoiseau, D., Marsac, R., Vaňková, Z. and Komárek, M., 2021. Cadmium isotope fractionation during complexation with humic acid. Environ. Sci. Technol. 55, 7430-7444. https://doi.org/10.1021/acs.est.1c00646

Ravel, B. and Newville, M., 2005. Athena, Artemis, Hephaestus: Data analysis for X-ray absorption spectroscopy using IFEFFIT. J. Synchrotron Radiat. 12, 537-541. https://doi.org/doi:10.1107/S0909049505012719

Rehkämper, M., Wombacher, F., Horner, T. and Xue, Z., 2011. Natural and anthropogenic Cd isotope variations, in: Baskaran, M. (Ed.), Handbook of environmental isotope geochemistry. Springer, Berlin Heidelberg, pp. 125-154.

Saldi, G.D., Noireaux, J., Louvat, P., Faure, L., Balan, E., Schott, J. and Gaillardet, J., 2018. Boron isotopic fractionation during adsorption by calcite – Implication for the seawater pH proxy. Geochim. Cosmochim. Acta 240, 255-273. https://doi.org/10.1016/j.gca.2018.08.025

Schauble, E.A., 2004. Applying stable isotope fractionation theory to new systems. Rev. Mineral. Geochem. 55, 65-111. https://doi.org/10.2138/gsrmg.55.1.65

Shirvani, M., Kalbasi, M., Shariatmadari, H., Nourbakhsh, F. and Najafi, B., 2006a. Sorption–desorption of cadmium in aqueous palygorskite, sepiolite, and calcite suspensions: Isotherm hysteresis. Chemosphere 65, 2178-2184. https://doi.org/10.1016/j.chemosphere.2006.06.002

Shirvani, M., Shariatmadari, H., Kalbasi, M., Nourbakhsh, F. and Najafi, B., 2006b.

817 Sorption of cadmium on palygorskite, sepiolite and calcite: Equilibria and
818 organic ligand affected kinetics. Colloids Surf. A Physicochem. Eng. Asp. 287,
819 182-190. https://doi.org/10.1016/j.colsurfa.2006.03.052
820 Smrzka, D., Zwicker, J., Bach, W., Feng, D., Himmler, T., Chen, D. and Peckmann, J.,
821 2019. The behavior of trace elements in seawater, sedimentary pore water, and
822 their incorporation into carbonate minerals: A review. Facies 65, 41.
823 https://doi.org/10.1007/s10347-019-0581-4
824 Spadini, L., Manceau, A., Schindler, P.W. and Charlet, L., 1994. Structure and
825 stability of Cd^{2+} surface complexes on ferric oxides: 1. Results from EXAFS
826 spectroscopy. J. Colloid Interface Sci. 168, 73-86.
827 https://doi.org/10.1006/jcis.1994.1395
828 Sun, Q., Cui, P.-X., Fan, T.-T., Wu, S., Zhu, M., Alves, M.E., Zhou, D.-M. and Wang,
829 Y.-J., 2018. Effects of Fe(II) on Cd(II) immobilization by Mn(III)-rich δ-MnO_2.
830 Chem. Eng. J. 353, 167-175. https://doi.org/10.1016/j.cej.2018.07.120
831 Sun, Q., Cui, P.-X., Zhu, M., Fan, T.-T., Ata-Ul-Karim, S.T., Gu, J.-H., Wu, S., Zhou,
832 D.-M. and Wang, Y.-J., 2019a. Cd(II) retention and remobilization on δ-MnO_2
833 and Mn(III)-rich δ-MnO_2 affected by Mn(II). Environ. Int. 130, 104932.
834 https://doi.org/10.1016/j.envint.2019.104932
835 Sun, Q., Liu, C., Cui, P., Fan, T., Zhu, M., Alves, M.E., Siebecker, M.G., Sparks, D.L.,
836 Wu, T., Li, W., Zhou, D. and Wang, Y., 2019b. Formation of Cd precipitates on
837 γ-Al_2O_3: Implications for Cd sequestration in the environment. Environ. Int.
838 126, 234-241. https://doi.org/10.1016/j.envint.2019.02.036

839 Sweere, T.C., Dickson, A.J., Jenkyns, H.C., Porcelli, D. and Henderson, G.M., 2020.
840 Zinc- and cadmium-isotope evidence for redox-driven perturbations to global
841 micronutrient cycles during Oceanic Anoxic Event 2 (Late Cretaceous). Earth.
842 Planet. Sci. Lett. 546, 116427. https://doi.org/10.1016/j.epsl.2020.116427
843 Tiberg, C. and Gustafsson, J.P., 2016. Phosphate effects on cadmium(II) sorption to
844 ferrihydrite. J. Colloid Interface Sci. 471, 103-111.
845 https://doi.org/10.1016/j.jcis.2016.03.016
846 Tribovillard, N., Algeo, T.J., Lyons, T. and Riboulleau, A., 2006. Trace metals as
847 paleoredox and paleoproductivity proxies: An update. Chem. Geol. 232, 12-32.
848 https://doi.org/10.1016/j.chemgeo.2006.02.012
849 Vasconcelos, I.F., Haack, E.A., Maurice, P.A. and Bunker, B.A., 2008. EXAFS
850 analysis of cadmium(II) adsorption to kaolinite. Chem. Geol. 249, 237-249.
851 https://doi.org/10.1016/j.chemgeo.2008.01.001
852 Wasylenki, L.E., Schaefer, A.T., Chanda, P. and Farmer, J.C., 2020. Differential
853 behavior of tungsten stable isotopes during sorption to Fe versus Mn
854 oxyhydroxides at low ionic strength. Chem. Geol. 558, 119836.
855 https://doi.org/10.1016/j.chemgeo.2020.119836
856 Wasylenki, L.E., Swihart, J.W. and Romaniello, S.J., 2014. Cadmium isotope
857 fractionation during adsorption to Mn oxyhydroxide at low and high ionic
858 strength. Geochim. Cosmochim. Acta 140, 212-226.
859 https://doi.org/10.1016/j.gca.2014.05.007
860 Wiederhold, J.G., 2015. Metal stable isotope signatures as tracers in environmental

geochemistry. Environ. Sci. Technol. 49, 2606-2624. https://doi.org/10.1021/es504683e

Wombacher, F., Rehkämper, M., Mezger, K. and Münker, C., 2003. Stable isotope compositions of cadmium in geological materials and meteorites determined by multiple-collector ICPMS. Geochim. Cosmochim. Acta 67, 4639-4654. https://doi.org/10.1016/S0016-7037(03)00389-2

Xie, X., Yan, L., Li, J., Guan, L. and Chi, Z., 2020. Cadmium isotope fractionation during Cd-calcite coprecipitation: Insight from batch experiment. Sci. Total Environ. 760, 143330. https://doi.org/10.1016/j.scitotenv.2020.143330

Yan, X., Zhu, M., Li, W., Peacock, C.L., Ma, J., Wen, H., Liu, F., Zhou, Z., Zhu, C. and Yin, H., 2021. Cadmium isotope fractionation during adsorption and substitution with iron (oxyhydr)oxides. Environ. Sci. Technol. 55, 11601-11611. https://doi.org/10.1021/acs.est.0c06927

Ye, Z., Zhou, J., Liao, P., Finfrock, Y.Z., Liu, Y., Shu, C. and Liu, P., 2022. Metal (Fe, Cu, and As) transformation and association within secondary minerals in neutralized acid mine drainage characterized using X-ray absorption spectroscopy. Appl. Geochem. 139, 105242. https://doi.org/10.1016/j.apgeochem.2022.105242

Yuan, W., Saldi, G.D., Chen, J., Vetuschi Zuccolini, M., Birck, J.-L., Liu, Y. and Schott, J., 2018. Gallium isotope fractionation during Ga adsorption on calcite and goethite. Geochim. Cosmochim. Acta 223, 350-363. https://doi.org/10.1016/j.gca.2017.12.008

883 Zachara, J.M., Cowan, C.E. and Resch, C.T., 1991. Sorption of divalent metals on
884 calcite. Geochim. Cosmochim. Acta 55, 1549-1562.
885 https://doi.org/10.1016/0016-7037(91)90127-Q
886 Zachara, J.M., Kittrick, J.A. and Harsh, J.B., 1988. The mechanism of Zn^{2+} adsorption
887 on calcite. Geochim. Cosmochim. Acta 52, 2281-2291.
888 https://doi.org/10.1016/0016-7037(88)90130-5
889 Zeebe, R.E., 2012. History of seawater carbonate chemistry, atmospheric CO_2, and
890 ocean acidification. Ann. Rev. Earth Planet. Sci. 40, 141-165.
891 https://doi.org/10.1146/annurev-earth-042711-105521
892 Zhang, Y., Wen, H., Zhu, C., Fan, H. and Cloquet, C., 2018. Cadmium isotopic
893 evidence for the evolution of marine primary productivity and the biological
894 extinction event during the Permian-Triassic crisis from the Meishan section,
895 South China. Chem. Geol. 481, 110-118.
896 https://doi.org/10.1016/j.chemgeo.2018.02.005
897 Zhao, Y., Li, Y., Wiggenhauser, M., Yang, J., Sarret, G., Cheng, Q., Liu, J. and Shi, Y.,
898 2021. Theoretical isotope fractionation of cadmium during complexation with
899 organic ligands. Chem. Geol. 571, 120178.
900 https://doi.org/10.1016/j.chemgeo.2021.120178
901 Zhou, Z., Liu, P., Wang, S., Finfrock, Y.Z., Ye, Z., Feng, Y. and Li, X., 2022.
902 Iron-modified biochar-based bilayer permeable reactive barrier for Cr(VI)
903 removal. J. Hazard. Mater. 439, 129636.
904 https://doi.org/10.1016/j.jhazmat.2022.129636

905